ADVANCED ENERGY MATERIALS
www.advenergymat.de

Thickness Insensitive Organic Solar Cells with High Figure-of-Merit-X Enabled by Simultaneous D/A Interpenetration and Stratification

Xiyun Xie, Ruijie Ma, Yongmin Luo, Top Archie Dela Peña, Patrick Wai-Keung Fong, Dou Luo, Hrisheekesh Thachoth Chandran, Tao Jia, Mingjie Li, Jiaying Wu,* Aung Ko Ko Kyaw,* and Gang Li**

Low cost and printing friendly fabrication of organic solar cells (OSCs) require thick-film devices with simply structured photoactive molecules. Thus, achieving high power conversion efficiency (PCE) for non-fused ring acceptor-based devices with high thickness is of great significance. Herein, by transforming traditional blend casting method to emerging sequential deposition (SD) method, D18:A4T-16 active blend exhibits large efficiency improvement from 8.02% to 14.75% in 300 nm thick devices. Systematic morphological and photophysical characterizations showcase the effectiveness of SD processing in achieving sufficient donor/acceptor interpenetration and vertical stratification, which eliminates the dilemma of charge generation/transport in blend casting films. Meanwhile, D18 bottom layer is proven helpful in realizing fast evaporation of postdeposited poor solvent, resulting in naturally thickened active layer with well-regulated crystallization. Furthermore, a new index to emphasize thick-film devices based on nonfused ring acceptors, called figure-of-merit-X (FoM-X), has been defined. The SD processed D18:A4T-16 devices herein, with 300 nm, 500 nm, and 800 nm thicknesses possess leading FoM-X values.

1. Introduction

Though organic solar cells (OSCs) are approaching 20% power conversion efficiency (PCE) in single-junction devices, the production cost of these high-efficiency systems to an economically practical level is not proven, due to the undesirable synthetic complexity (SC) of fused ring molecular acceptors.[1–17] Up to now, only a few cases have realized satisfactory figure-of-merits (FoMs) with high PCEs.[18–26] On the other hand, efficiency pursuit efforts are usually paid for thin-film (≈100 nm active layer) devices, but >300 nm thickness active layer based device results are more instructive for next stage roll-to-roll printing fabrication.[27–34] Thereby, the field urgently needs corresponding contributions on high-performing thick-film (≥300 nm) non-fused ring molecular acceptor based OSCs, but such devices with high efficiency are rare.[35]

Compared to fused ring counterparts, non-fused small molecules connected by C—C bonds are in nature of poorer planarity and rigidity, thereby insufficient intramolecular charge transfer, usually leading to unsatisfactory exciton generation. Furthermore, according to our recent understanding on the correlation between the exciton diffusion length versus pure phase length scale ($L_D/2R_g$) and charge generation, in bulk heterojunction (BHJ) scene, enlarged domain size of non-fused acceptor is not suggested.[36] However, the thick-film

X. Xie, R. Ma, P. W.-K. Fong, H. T. Chandran, G. Li
Department of Electrical and Electronic Engineering
Research Institute for Smart Energy (RISE)
Photonic Research Institute (PRI)
The Hong Kong Polytechnic University
Hong Kong 999077, China
E-mail: ruijie.ma@polyu.edu.hk; gang.w.li@polyu.edu.hk

The ORCID identification number(s) for the author(s) of this article can be found under https://doi.org/10.1002/aenm.202401355

DOI: 10.1002/aenm.202401355

X. Xie, D. Luo, A. K. K. Kyaw
Guangdong University Key Laboratory for Advanced Quantum Dot Displays and Lighting Department of Electrical & Electronic Engineering
Guangdong University Key Laboratory for Advanced Quantum Dot Displays and Lighting, Department of Electronic & Electrical Engineering
Southern University of Science and Technology
Shenzhen 518055, China
E-mail: aung@sustech.edu.cn

Y. Luo, T. A. Dela Peña, J. Wu
Function Hub
Advanced Materials Thrust
The Hong Kong University of Science and Technology
Nansha Guangzhou 511400, China
E-mail: jiayingwu@ust.hk

devices of high PCEs have been proven containing large-size crystallites/aggregates in films, particularly for small molecular acceptors.[37–41] Accordingly, traditional blend cast deposition for active layer is not applicable in boosting efficiency on thick-film devices of non-fused ring acceptors.

In recent years, utilizing sequential deposition (SD) of donor layer and acceptor layer has been an emerging fabrication method to realize highly efficient and reproducible devices, due to well-defined vertical donor–acceptor (D/A) phase separation, and more uniformed film quality.[42–53] This method has been shown effective in promoting thick-film device's PCE, yet efficiency loss is still significant compared to thin-film ones due to more severe exciton recombination.[54–56] In view of this, SD treatment is a promising candidate to achieve thick-film non-fused OSC's efficiency breakthrough, once more sophisticated optimization is carried out to further suppress the recombination.

From the material library, D18 is chosen as the donor material in our work since its strong crystallinity and good compatibility with non-fused ring acceptors, to match with A4T-16, which is well studied by us and revealed performing well by o-xylene plus 1,8-diiodooctane (XY+DIO) cosolvent processing.[57–62] To better compare the performance, here we define a new index called figure-of-merit-X (FoM-X = FoM*(d/100 nm)), where d is the thickness of active layer. The D18:A4T-16 blend is firstly studied by blend cast in 100 nm and 300 nm thickness scenarios. The results demonstrate that best PCE of 12.04% is achieved by 100 nm device, while 300 nm cell yields only 9.04%. The sacrificed open-circuit voltage (V_{OC}), short-circuit current density (J_{SC}), and fill factor (FF) show film thickening is detrimental to charge generation and collection as predicted. On the other hand, the SD method is applied, i.e., casting chloroform (CF) dissolved D18 solution before casting A4T-16 (in XY+DIO). Surprisingly, SD devices with 60 nm D18 layer exhibit insignificant performance change with 40 nm to 240 nm A4T-16 layer atop (15.08% vs 14.75%). When increasing D18 layer's thickness to 180 nm, and decreasing acceptor layer to 120 nm, the efficiency goes back to 10.24%, which is again caused by simultaneous loss in V_{OC}, J_{SC}, and FF. Subsequently, morphological and photophysical characterizations reveal that SD photoactive layers contain sufficient D/A interface for charge separation and well-regulated crystalline features. Then the effectiveness of D/A interpenetration and stratification required SD method is extended to D18:BTP-eC9 by the same fabrication recipe, resulting in 17.00% and 12.53% PCEs for 300 nm and 500 nm devices. Our work presents a novel strategy and in-depth understanding for efficiency boosting on thick-film OSCs, a new concept to evaluate device performance, and a breakthrough for non-fused ring OSC systems.

T. A. Dela Peña, M. Li
Department of Applied Physics
The Hong Kong Polytechnic University
Hong Kong 999077, China
T. Jia
School of Optoelectronic Engineering
Guangdong Polytechnic Normal University
Guangzhou 510665, China

2. Results and Discussion

D18 and A4T-16′s chemical structures are illustrated in **Figure 1**, together with the temperature-dependent aggregation (TDA) feature of D18, and the SD processing schematic diagram. The solubility of D18 has been confirmed extremely poor in ortho-xylene (XY), and even in CF it requires high temperature to be dissolved.[63,64] Here this feature is also evaluated. By simultaneously increasing the heating temperature to 100 °C and stirring, the D18 can be dissolved within 20 mins and demonstrates light red. When cooling down the solution to room temperature (RT), it appears darker and stickier, indicating much stronger chain entanglement and aggregation. After being reheated to 100 °C, it turns to be light red and more fluidic again. Thereby, post-deposited acceptor layer with XY as solvent will not cause small molecules fully interpenetrating the donor layer due to D18's poor solubility, thus significant vertical donor-acceptor stratification can be obtained. This prediction is substantiated by the time-of-flight secondary ion mass spectroscopy (ToF-SIMS) experiment results, as demonstrated in Figure S1 (Supporting Information).

Next, the morphology study is carried out on both BHJ blend casting and SD processed films with different thicknesses by ultraviolet–visible (UV–vis) absorption spectroscopy and atomic force microscopy (AFM) measurements, as displayed in Figure S2 (Supporting Information). Shown in Figure S2a (Supporting Information), D18's optical property is not altered significantly by XY+DIO washing, supporting the declaration of post casting will not induce strong swelling-intercalation-phase separation (SIPS) phenomenon in this system, thus significant stratification and partial donor–acceptor interpenetrating region providing sufficient interface for charge separation.[50] The AFM images supports that D18's surface morphology (aggregation in bulk can be inferred) is not changed by solvent washing. Furthermore, it shows A4T-16 neat film cast from XY+DIO solvent has very large aggregates, with significant 0–0 and 0–1 vibrational peak in its absorption profile. When blending with D18 and cast by CF, A4T-16 demonstrates no significant aggregation feature according to both absorbances and AFM images, until the participation of DIO comes. Empirically, more significant aggregation features represent more suitable phase separation, which is beneficial to charge transport, thus higher FF. For SD processed films, the normalized absorption profiles show identical shapes in acceptor region, demonstrating similar aggregation behaviors of the A4T-16 molecules. The D18's relative absorption intensity of 60 + 240 nm combination is much lower than others, supporting A4T-16 content is clearly more than D18 in this film. By comparing the absorption edges of these films with that of A4T-16′s neat film, blueshift phenomenon is obvious, suggesting bottom layered D18 can suppress the undesirable over aggregation of small molecule acceptors induced by DIO. This is also supported by AFM images, where their surface roughness values, root mean squares (RMSs), are apparently lower than A4T-16 neat film, and large aggregates in neat film are replaced with well separated small clusters. In addition, it is noteworthy that all blend films fail in realizing fibrillar network dominated morphology, unlike current high-performance systems.[65–67] Thereby, blend cast active layers would face the dilemma of contradicting phase separation behavior.[36]

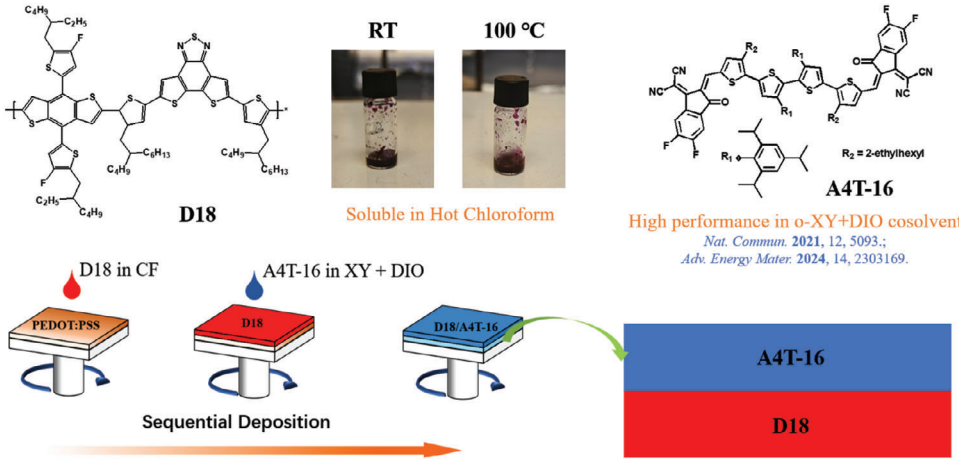

Figure 1. General information of materials and device fabrication. Device structures of D18 and A4T-16; photos of 5 mg mL^{-1} D18 dissolved in CF under room temperature (cooled from 100 °C) and 100 °C (reheated); the schematic diagram of SD processing.

Next, the crystalline characteristics of blend cast and SD films are investigated by utilizing grazing incidence wide-angle X-ray scattering (GIWAXS) test.[68–71] In **Figure 2** and Figure S3 (Supporting Information), the 2D patterns for neat films, SD films and blend films are displayed, while the corresponding extracted line-cut profiles alongside in-plane (IP) and out-of-plane (OOP) directions are given in Figure S4 (Supporting Information). To evaluate the vertical crystallization differences of SD devices, a smaller grazing incidence angle of 0.1° is applied. In addition, the calculated characteristic peak properties are summarized in Tables S1 and S2 (Supporting Information) for IP lamellar peak and OOP π–π stacking peak, respectively. Accordingly, D18 has a face-on orientation dominant packing motif, suggested by its clear OOP (010) peak signal, and significant IP lamellar packing. On the other hand, neat film A4T-16 demonstrates multiple diffraction peaks of ring shape, which indicates its poor molecular packing order and random orientation. Specifically, an IP directional (010) peak and ring-shaped lamellar signal at $q \approx 0.5$ $Å^{-1}$ are found to be A4T-16's unique packing characteristics. XY+DIO cosolvent washing leads to insignificant decrease of crystallinity and packing order of D18, which is consistent with above conclusions. The BHJ film's results suggest blending with D18, the crystalline features of A4T-16 would be diminished. For both 100 and 300 nm film, DIO treatment leads to partial A4T-16's independent crystallization, evidenced by π–π stacking peak splitting and ring-like diffraction signal's reappearance (Figure S3, Supporting Information). Parallelly, SD processed films are evaluated: i) 60 + 40 nm active layer shows well intermixed crystalline features at upper part, where (010) peak locates at 1.85 $Å^{-1}$, while the general film's signal suggests independent donor and acceptor crystallization (π–π stacking peaks are at 1.74 and 1.93 $Å^{-1}$); ii) 60 + 240 nm film's signals detected by 0.1° and 0.25° are all mainly from A4T-16 due to their (010) peak position are highly similar to those of neat film A4T-16; iii) 180 + 120 nm instead, displays significant D18's crystalline feature when detected by 0.25° incidence. These results well support that SD processed active layers simultaneously possess sufficient D/A intermixing and vertical segregation. In addition, it is also defended SD processed thick film contain highly ordered packing A4T-16 molecular clusters with clear face-on orientation, which is beneficial to maintaining efficient charge transport. The mobility evaluation further supports this declaration. The space-charge-limited-current (SCLC) method is utilized to extract hole mobility (μ_h) and electron mobility (μ_e) values, from hole-only and electron-only device results (Figure S5, Supporting Information). Then, the calculated mobilities are summarized in Table S3 (Supporting Information). The μ_h and μ_e values of SD devices are stably at a normal level, guaranteeing the charge transport.

Moreover, the practicability of constructing such thick acceptor layer is evaluated by using in situ UV–vis absorption measurement.[72–74] By screening the whole process of casting A4T-16's XY+DIO cosolvent onto PEDOT:PSS and D18 films, it can be found that acceptor layer's solidification and aggregation behaviors. The details are visualized in Figure 2b, where three stages for liquid to solid transition of A4T-16 can be found when casting onto PEDOT:PSS: I) solvent evaporation (4.5s) with A4T-16 small molecules forming clusters; II) the absorption red shift due to continuous molecular aggregation (10.3s); III) absorption weakening caused by thickness loss (7.3s). Meanwhile, there's only stage I (7.5s) can be marked for D18 substrate. This difference is supposed to be made by D18's surface roughness, which limits the solvent removal by centrifugal effect, thus more A4T-16 materials are left on substrates. Besides, this process is also beneficial to suppressing A4T-16's aggregation degree, substantiating the disappearance of neat film's large aggregates in SD processed films.

Solar cells were fabricated of ITO/PEDOT:PSS/active layer/PFN-Br/Ag structure, and their current density versus voltage (J–V) characteristics are plotted in Figure S4 (Supporting Information), with deduced photovoltaic parameters summarized in Table S4 (Supporting Information). Then the parameter's variation tendency is visualized in **Figure 3**a, where high thickness tolerance of 60 nm D18 bottom layer-based SD devices is directly presented. On the contrary, within fixed total thickness of 300 nm, increasing D18 layer's thickness from 60 to 180 nm, the PCE keeps dropping from 14.75% to 10.24%, due to ceaselessly decreased V_{OC}, J_{SC}, and FF. Meanwhile, the CF blend cast

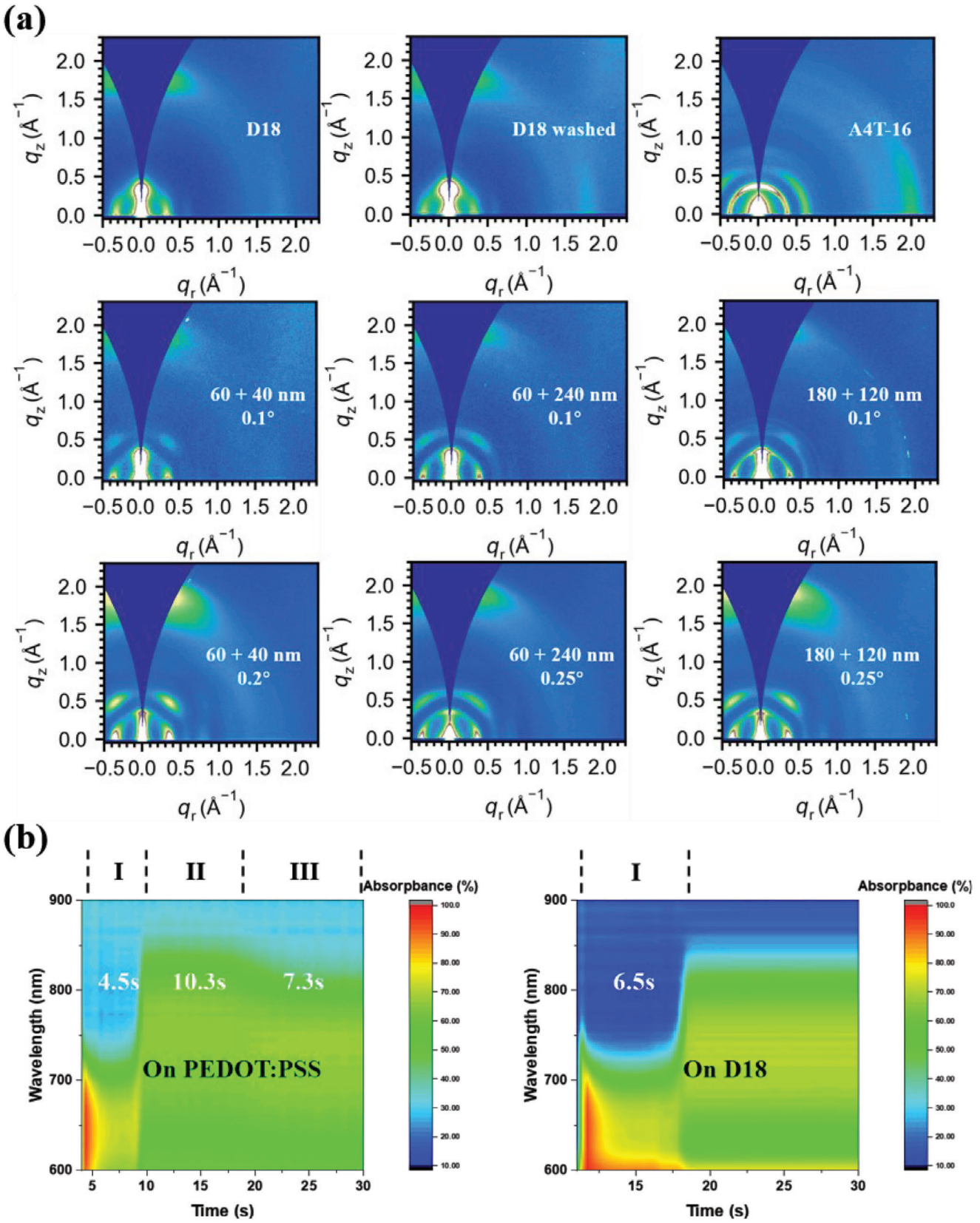

Figure 2. Morphology features. a) 2D GIWAXS patterns of neat films and varied angle detected SD films. b) In situ absorption spectra of A4T-16 solution cast on the PEDOT:PSS and D18 films, that are marked with crystallization stages and periods.

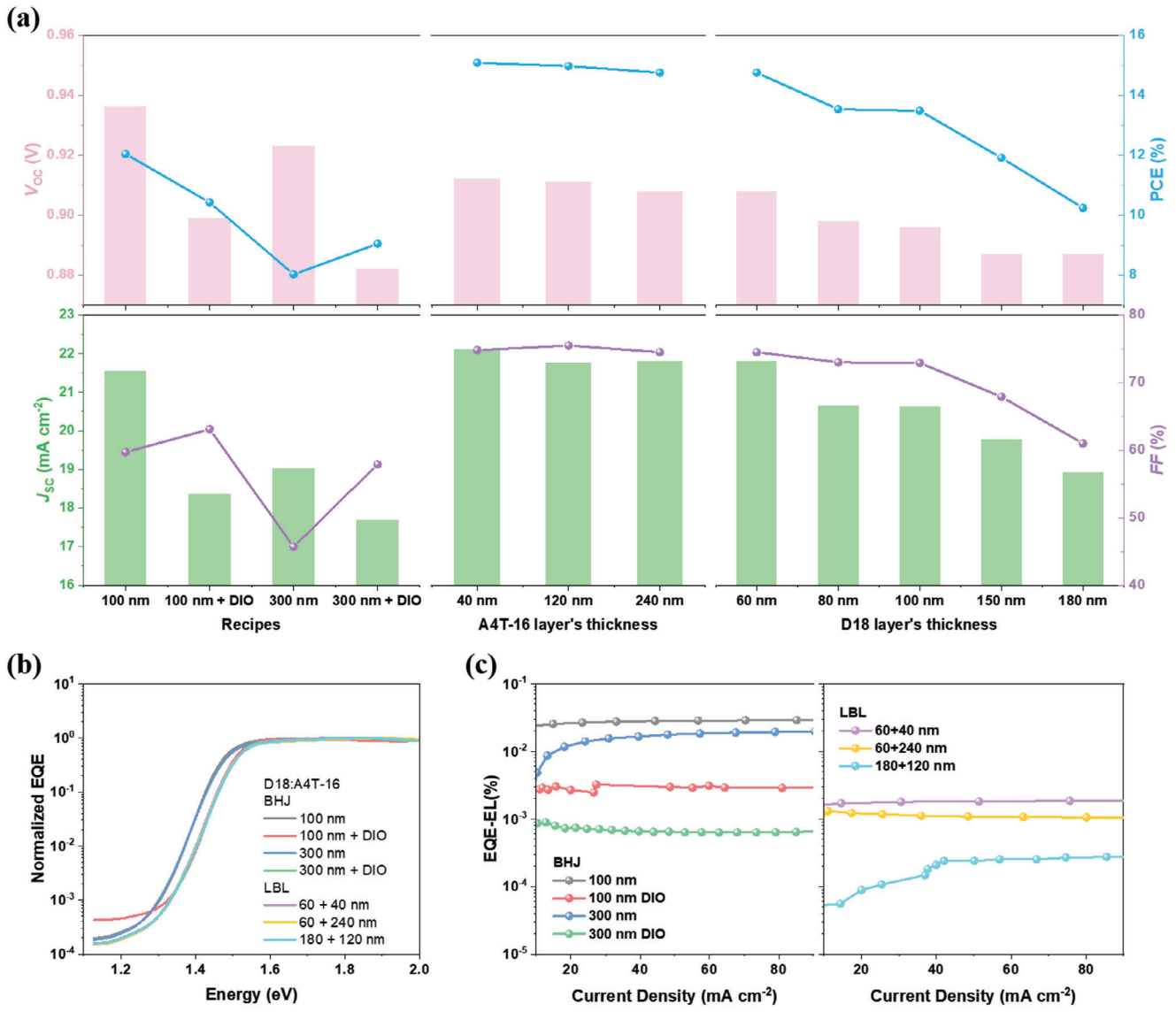

Figure 3. Photovoltaic performance. a) Device parameter variations of D18:A4T-16 system processed by blend casting and SD. b) FTPS-EQE spectra and c) EQE-EL results for representative blend casting and SD devices.

D18:A4T-16 devices exhibits best efficiency of 12.04% in 100 nm layer without DIO treatment thanks to high V_{OC} and J_{SC}, though FF is poor. After treated by DIO in precursor, 100 nm blend cast device displays only 10.42% PCE due to significant loss in V_{OC} and J_{SC}, which cannot be saved by increased FF. Correlated with the morphology analysis, it clearly reflects the dilemma of enlarging or minimizing phase separation length scale. The 300 nm blend cast device exhibits more significant FF loss, due to the lack of continuous pure phase. In this scenario, precursor treated by DIO leads to better PCE (9.04% vs 8.02%) due to FF recovery. Reasonably, severe V_{OC} and J_{SC} reduction is observed, as well. Subsequently, the external quantum efficiency (EQE) spectra of all devices are measured at shown in Figure S6 (Supporting Information), too. The derived measurement error for optimal devices is found smaller than 5%. Noteworthy, the DIO-processed devices, regardless of blend casting or SD ones, display blueshift EQE edges compared with those without DIO, corresponding to wider bandgap ($E_{g\text{-}PV}$), but containing clearly lower V_{OC} values. Hence, an energy loss (E_{loss}) study is implemented by applying sensitive EQE (s-EQE) and electroluminescence (EL) measurements upon representative devices. The normalized EQE spectra are put in Figure 3b, and EQE-EL results are placed in Figure 3c. The derived parameters are displayed in Table S5 (Supporting Information). The results suggest that enlarged E_{loss} mainly comes from increased non-radiative energy loss (ΔE_3), which is observed being increased by two factors: film thickening and DIO treatment. In SD processed devices, D18 layer's thickening is more powerful in raising ΔE_3 than that of A4T-16 layer.

Following addressing V_{OC} concerns, device physics side analyses for understanding on J_{SC} and FF change are carried out. The charge dissociation and collection behaviors are evaluated by photocurrent density versus effective voltage (J_{ph} vs V_{eff})

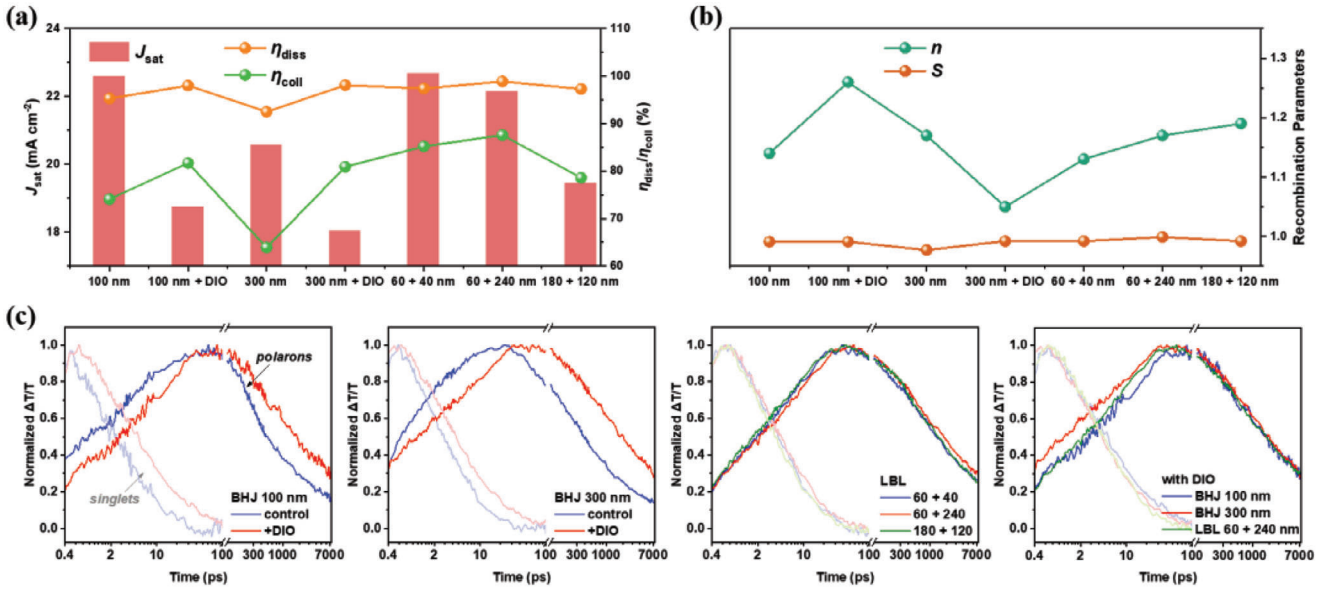

Figure 4. Charge behaviors and carrier dynamics. a) Summary of charge dissociation/collection parameters: J_{sat}, η_{diss}, and η_{coll}. b) The change of n (trap-assisted recombination) and S (bimolecular recombination). c) Picosecond to sub-nanosecond singlet and polaron dynamics: parallel comparisons of featured solar cells.

relationships. The experimental details, resulting curves (Figure S7, Supporting Information), and calculation processes are elaborated in Supporting Information. Key parameters including saturated current density (J_{sat}), charge dissociation efficiency (η_{diss}), and collection efficiency (η_{coll}) are presented in **Figure** 4a. Both blend casting and SD processed active layers exhibit over 22.5 mA cm^{-2} J_{sat} when thickness locates at 100 nm. Increasing A4T-16 layer thickness can maintain the J_{sat} > 22 mA cm^{-2}, while raising D18 layer's thickness is significantly harmful for this value. Besides, DIO treatment and film thickening are negative to this index. These changes are well consistent with above discussed morphology evolutions. In addition, the changing characteristics of η_{diss} and η_{coll} are supportive to FF variation and phase segregation (horizontally and vertically), too. Afterwards, the recombination degrees are assessed by using J–V measurement under various illumination intensities. Corresponding V_{OC}/J_{SC} versus P_{light} curves are plotted in Figure S8 (Supporting Information). Related fitting methods and physical meanings are presented in Supporting Information, as well. The ideal factor n (for trap-assisted & surface recombination) and bimolecular recombination index S are derived and drawn in Figure 4b.[75] Blend cast 100 nm and 300 nm systems have a similar degree of trap related and surface recombination, while DIO treatment is responsible for largely increasing traps in 100 nm layer, but more efficient in leading to surface recombination sites in 300 nm ones. As for SD cast devices, the traps marginally increase with the increase of thickness. Thicker D18 bottom layer results in more traps than A4T-16 top layer thickening does. All above parameters can be found in Table S6 (Supporting Information).

Subsequently, the exciton splitting and recombination kinetics at the donor/acceptor interface are studied by applying femto-second transient absorption spectroscopy (fs-TAS) technology.[76–79] The blend films with different processing recipes are excited by 800 nm laser with low pump fluence of 3 μJ cm^{-2}. Acquired results presented as contour maps and spectral line cuts are displayed in Figures S9 and S10 (Supporting Information). The acceptor singlet exciton kinetics are obtained from the decay of acceptor ground-state-bleach (GSB) signals, while the polaron's increasing and decreasing trends extracted from hole polarons photobleaching (PB), which corresponds to the donor absorption range, are used to describe the free charge generation and sub-nano second recombination behavior (i.e., mainly pertaining to the initial recombination of free charges formed at the donor/acceptor interfaces). The decay curves are shown by groups in Figure 4c. First, by comparing blend cast devices, DIO's tuning effect upon exciton behavior is identical to our previous finding: slower kinetics for singlet exciton dissociation, polarons generation, and polarons recombination. Considering the enlarged phase separation scale imparting sacrificed donor/acceptor interface area, the reduction of J_{SC} and enhancement of FF are well supported. On the contrary, by comparing SD processed devices of D18/A4T-16 thicknesses of 60/40, 60/240, and 180/120 nm demonstrates nearly identical exciton behaviors. Thereby, the donor/acceptor interface property of SD type films, no matter what thicknesses are, is highly similar. One step further, 60/240 nm SD film's kinetics curve is selected to compare with those of DIO-treated 100 and 300 nm blend cast active layers. This is designed to further clarify the donor/acceptor interface's property differences of SD and blend cast devices by expelling out the effect of DIO treatment. As a result, the polaron recombination dynamics of the three systems are almost identical, but there exist definable free charge generation kinetics differences ($k_{100nm} < k_{60+240nm} < k_{300nm}$). Based on such results, DIO treatment can tune the D/A interface energy landscape by modulating A4T-16's crystallization characteristics. D18 is not affected by DIO's addition, thus charge generation kinetics differences show up, which is caused by morphology change between blend casting

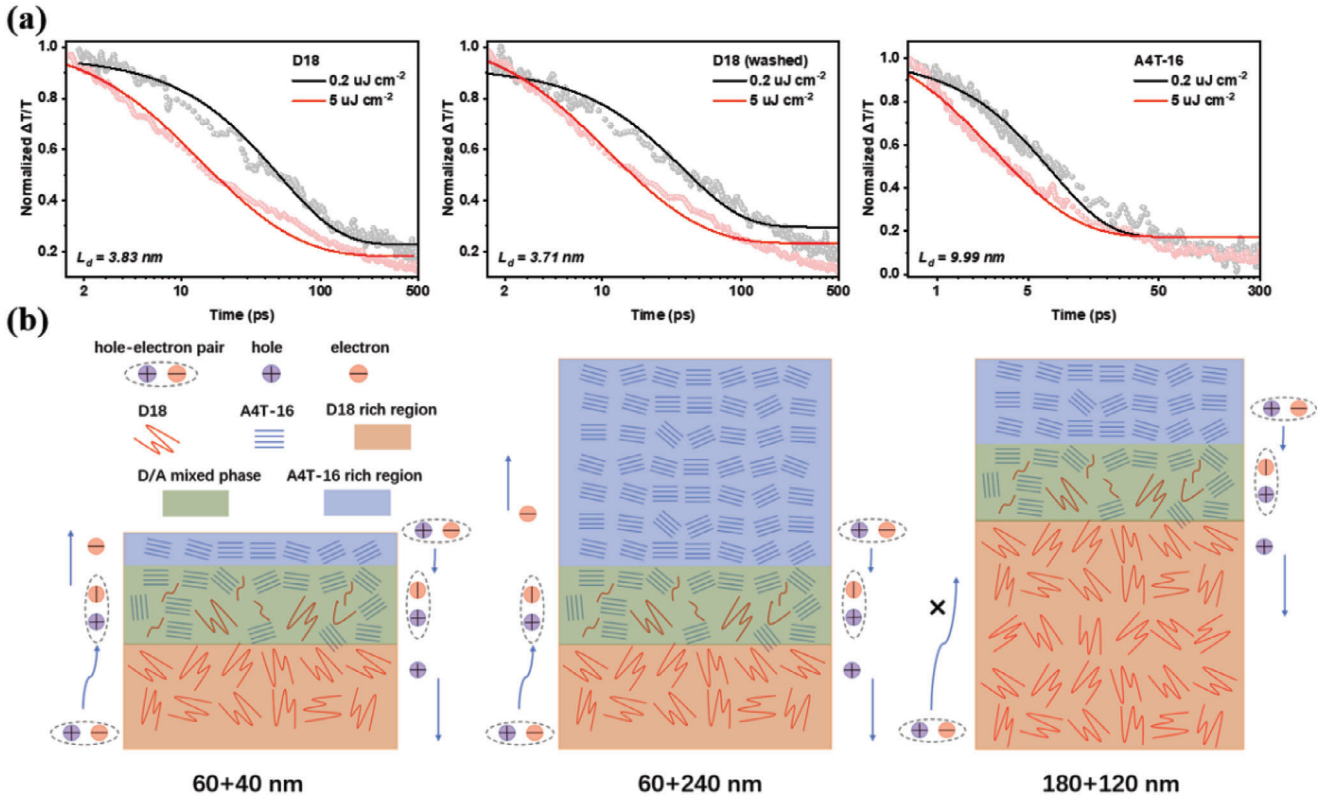

Figure 5. Exciton diffusion length evaluation and proposed working mechanism. a) Singlet exciton decay curves of neat D18 and A4T-16 films excited at low and high pump fluences. b) Schematic diagram of charge generation and transport model of SD active layers with different donor and acceptor thicknesses.

and SD films. These phenomena indicate J_{SC} and FF differences among SD devices are mainly induced by charge recombination due to diffusion length (L_D) limited singlet exciton geminate loss.

The L_D assessment is realized by combining fs-TAS measurements under different fluences upon neat films (excited @400 nm for D18, @800 nm for A4T-16) and the exciton-exciton annihilation (EEA) models.[80,81] Extremely low fluence is necessary to estimate the intrinsic exciton lifetimes while high pump fluence can be used to estimate L_D based on the EEA behavior. According to **Figure 5a**, The L_D values of D18 (as cast), D18 (washed), and A4T-16 are 3.83, 3.71, and 9.99 nm, respectively. With such low L_D, it is reasonable that monomolecular (geminate) recombination would be serious once D18's thickness gets larger.

With above characterizations, the working mechanism of SD type solar cells can be illustrated by what is portrayed in Figure 5b. Thanks to D18's absorption range, short-wavelength photons are almost converted to excitons in its bottom pure phase and top intermixing phase, while casting 40 nm A4T-16 is enough to absorb left photons of 600 to 850 nm wavelength. Accordingly, increasing A4T-16 layer's thickness is not harmful for exciton migrating to donor/acceptor interface for splitting, since thickened part does not absorb light. However, once increasing D18 layer's thickness elongated the required L_D for excitons equally, thus resulting in severe geminate recombination, negative for both J_{SC} and *FF* (**Table 1**).

To better evaluate the practical value of typical OSCs, a series of parameters derived from figure-of-merit (FoM) have been proposed in recent years, including the stability, fabrication cost, synthetic complexity, etc. as factors.[82,83] Herein, we define FoM-X = (PCE/SC)*(d/100 nm) to include the importance of increasing film thickness. We take our recent summary of SC values representative acceptors as the basic database (Table S7, Supporting Information), and then figure out the FoM and FoM-X values (Table S8, Supporting Information) for direct comparison.[23] In order to evaluate the general applicability of SD processing's donor/acceptor mixing and segregation behaviors, eC9 is chosen to fabricate identical architecture devices, due to its good compatibility with XY+DIO cosolvent and wide commercial availability, as demonstrated by **Figure 6a**.[3]

Table 1. Device performances.

D18:acceptors	V_{OC} [V]	J_{SC} [mA cm^{-2}]	FF [%]	PCE [%]
A4T-16				
500 nm	0.897	21.44/20.74	72.0	13.85
800 nm	0.888	19.87/19.05	68.3	12.05
eC9				
300 nm	0.838	27.35/26.57	74.1	17.00
500 nm	0.814	23.44/22.69	65.7	12.53

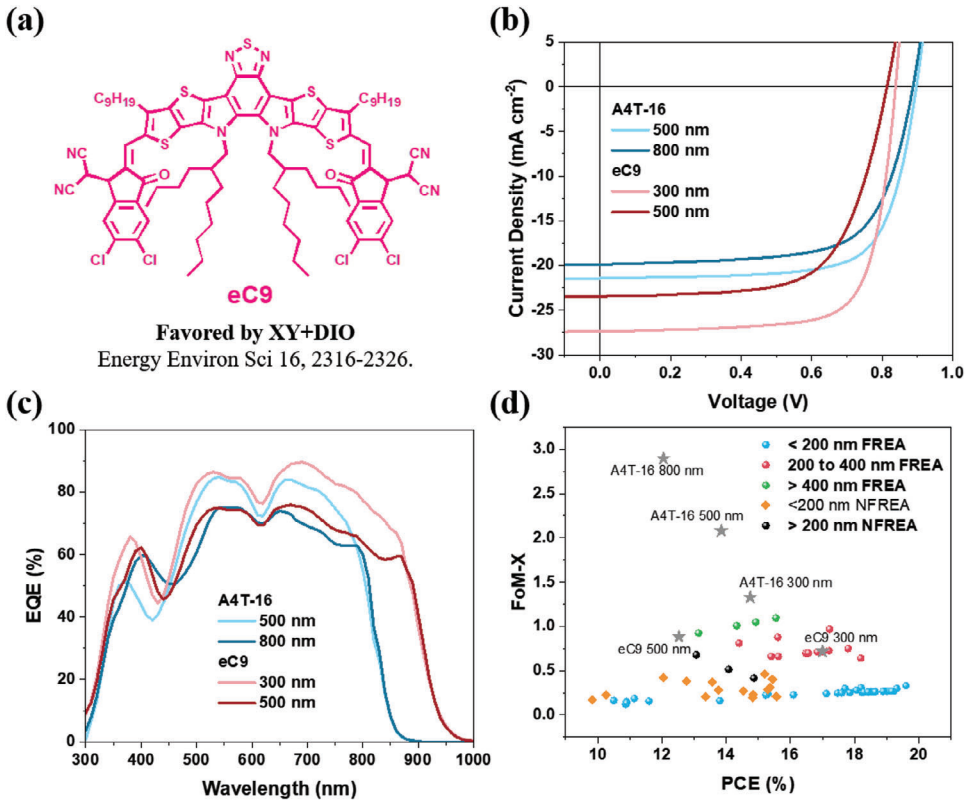

Figure 6. PCE and FoM-X pursuit. a) Chemical structure of eC9. b) *J–V* curves and c) EQE spectra of SD type devices with respective active layer thicknesses based on D18:A4T-16 and D18:eC9. d) A PCE versus FoM-X summary of this work and other reports.

Meanwhile, further exploration on thick-film D18:A4T-16 based devices are also carried out. The *J–V* curves and related EQE spectra of 500 nm, 800 nm D18:A4T-16, and 300 nm, 500 nm D18:eC9 are plotted in Figure 6b,c. As a result, 500 nm device (60 nm + 440 nm) exhibits 13.85% PCE, still a well-kept value. The efficiency drop of 800 nm device is due to concurrent reduction in V_{OC}, J_{SC} and FF, which might be the increase of traps in ultra-thick A4T-16 layer. The thickness tolerance of eC9 based devices are poorer, where 17.00% efficiency is given by 300 nm layer but only 12.53% PCE can be produced by 500 nm devices. This might be due to eC9 is more sensitive to DIO during liquid-to-solid crystallization. At last, the PCE versus FoM-X chart is portrayed based on literature results and SD processed device performances in this work. The representative high-performance fused ring acceptors related dots are denoted as FREA, while non-fused ones are named NFREA in Figure 6d. Apparently, thin-film FREA OSCs contain higher PCE but lower FoM-X than NFREA based ones. By increasing thickness, FoM-X values for D18:A4T-16 system effectively prove our design's advantage.

3. Conclusion

In summary, here we aim on constructing efficient organic solar cells (OSCs) based on low-cost non-fused ring acceptors with high active layer thickness, and compare the effectiveness of blend casting and SD processing. BHJ films exhibits poor performance for lack of fibrillar structures, while SD films with controlled donor layer thickness can realize high PCE with various acceptor layer thicknesses, thanks to simultaneous D/A intermixing and stratification. With the assistance of several morphological and device physics characterizations, the working mechanism of SD film's thickness insensitivity is demonstrated. Furthermore, by combining the perspectives of synthetic complexity and active layer thickness, a new index called FoM-X is defined, and our work is shown successful in achieving cutting-edge level FoM-X. Therefore, this study generates in-depth understanding in D/A interface behavior, SD type film's vertical segregation, and significant performance progress.

Supporting Information

Supporting Information is available from the Wiley Online Library or from the author.

Acknowledgements

G.L. acknowledges the support from Research Grants Council of Hong Kong (Project Nos 15221320, 15307922, C7018-20G, C5037-18G, C4005-22Y), RGC Senior Research Fellowship Scheme (SRFS2223-5S01), Shenzhen Science and Technology Innovation Commission (JCYJ20200109105003940), the Hong Kong Polytechnic University: Sir Sze-yuen Chung Endowed Professorship Fund (8-8480), RISE (Q-CDBK), PRI (Q-CD7X), and Guangdong-Hong Kong-Macao Joint Laboratory for Photonic-Thermal-Electrical Energy Materials and Devices (GDSTC No. 2019B121205001). R.M. thanks the PolyU Distinguished Postdoctoral Fellowship (1-YW4C). A.K.K.K. thanks the support from Shenzhen Science

Technology and Innovation Commission (JCYJ20220530113014033), the Natural Science Foundation of Guangdong Province (2024A1515010773), and the National Natural Science Foundation of China (Grant No. 62150610496). J.W. thanks the Guangdong government and the Guangzhou government for funding (2021QN02C110), the Guangzhou Municipal Science and Technology Project (No. 2023A03J0097 and No. 2023A03J0003), and NSFC (52303249); J.W. also thanks the support of HKUST Materials Characterization and Preparation Facility Guangzhou (MCPF-GZ).

Conflict of Interest

The authors declare no conflict of interest.

Author Contributions

X.X. and R.M. contributed equally to this work. X.X.: investigation, formal analysis, conceptualization, writing-original draft. R.M.: conceptualization, investigation, formal analysis, project administration, supervision, writing-review & editing. Y.L.: investigation, formal analysis. T.A.D.P.: investigation, formal analysis. P.W.-K.F.: investigation. D.L.: formal analysis. H.T.C.: investigation. T.J.: resources. J.W.: resources, supervision. A.K.K.K.: resources, supervision, funding acquisition, writing-review & editing. G.L.: conceptualization, resources, supervision, writing-review & editing, funding acquisition.

Data Availability Statement

The data that support the findings of this study are available from the corresponding author upon reasonable request.

Keywords

nonfused ring acceptor, organic solar cells, power conversion efficiency, sequential deposition, thick film

Received: March 25, 2024
Revised: June 2, 2024
Published online:

[1] J. Fu, Q. Yang, P. Huang, S. Chung, K. Cho, Z. Kan, H. Liu, X. Lu, Y. Lang, H. Lai, F. He, P. W. K. Fong, S. Lu, Y. Yang, Z. Xiao, G. Li, *Nat. Commun.* **2024**, *15*, https://doi.org/10.1038/s41467-024-46022-3.
[2] Z. Gan, L. Wang, J. Cai, C. Guo, C. Chen, D. Li, Y. Fu, B. Zhou, Y. Sun, C. Liu, J. Zhou, D. Liu, W. Li, T. Wang, *Nat. Commun.* **2023**, *14*, 6297.
[3] R. Ma, X. Jiang, J. Fu, T. Zhu, C. Yan, K. Wu, P. Müller-Buschbaum, G. Li, *Energy Environ. Sci.* **2023**, *16*, 2316.
[4] H. Lu, W. Liu, G. Ran, Z. Liang, H. Li, N. Wei, H. Wu, Z. Ma, Y. Liu, W. Zhang, X. Xu, Z. Bo, *Angew. Chem., Int. Ed.* **2023**, *62*, 202314420.
[5] J. Wang, Y. Wang, P. Bi, Z. Chen, J. Qiao, J. Li, W. Wang, Z. Zheng, S. Zhang, X. Hao, J. Hou, *Adv. Mater.* **2023**, *35*, 2301583.
[6] N. Su, J. Chen, M. Peng, G. Li, R. M. Pankow, D. Zheng, J. Ding, A. Facchetti, T. J. Marks, *J. Energy Chem.* **2023**, *79*, 321.
[7] B. Zou, W. Wu, T. A. Dela Peña, R. Ma, Y. Luo, Y. Hai, X. Xie, M. Li, Z. Luo, J. Wu, C. Yang, G. Li, H. Yan, *Nano-Micro Lett.* **2023**, *16*, 30.
[8] X. Xu, W. Jing, H. Meng, Y. Guo, L. Yu, R. Li, Q. Peng, *Adv. Mater.* **2023**, *35*, 2208997.
[9] W. Wu, Y. Luo, T. A. Dela Peña, J. Yao, M. Qammar, M. Li, H. Yan, J. Wu, R. Ma, G. Li, *Adv. Energy Mater.* **2024**, *14*, 2400354.
[10] K. Liu, Y. Jiang, G. Ran, F. Liu, W. Zhang, X. Zhu, *Joule* **2024**, *8*, 835.
[11] W. Wei, C. e. Zhang, Z. Chen, W. Chen, G. Ran, G. Pan, W. Zhang, P. Müller-Buschbaum, Z. Bo, C. Yang, Z. Luo, *Angew. Chem., Int. Ed.* **2024**, *63*, 202315625.
[12] H. Zhu, Y. Li, *Green Carbon* **2023**, *1*, 14.
[13] X. Wang, J. Wang, P. Wang, C. Han, F. Bi, J. Wang, N. Zheng, C. Sun, Y. Li, X. Bao, *Adv. Mater.* **2023**, *35*, 2305652.
[14] J.-W. Lee, C. Sun, J. Lee, D. J. Kim, W. J. Kang, S. Lee, D. Kim, J. Park, T. N.-L. Phan, Z. Tan, F. S. Kim, J.-Y. Lee, X. Bao, T.-S. Kim, Y.-H. Kim, B. J. Kim, *Adv. Energy Mater.* **2024**, *14*, 2303872.
[15] C. Wang, X. Ma, Y.-f. Shen, D. Deng, H. Zhang, T. Wang, J. Zhang, J. Li, R. Wang, L. Zhang, Q. Cheng, Z. Zhang, H. Zhou, C. Tian, Z. Wei, *Joule* **2023**, *7*, 2386.
[16] D. He, J. Zhou, Y. Zhu, Y. Li, K. Wang, J. Li, J. Zhang, B. Li, Y. Lin, Y. He, C. Wang, F. Zhao, *Adv. Mater.* **2024**, *36*, 2308909.
[17] S. Chen, S. Zhu, L. Hong, W. Deng, Y. Zhang, Y. Fu, Z. Zhong, M. Dong, C. Liu, X. Lu, K. Zhang, F. Huang, *Angew. Chem., Int. Ed.* **2024**, *63*, 202318756.
[18] Q. Bai, Q. Liang, H. Li, H. Sun, X. Guo, L. Niu, *Aggregate* **2022**, *3*, e281.
[19] G. Li, L.-W. Feng, S. Mukherjee, L. O. Jones, R. M. Jacobberger, W. Huang, R. M. Young, R. M. Pankow, W. Zhu, N. Lu, K. L. Kohlstedt, V. K. Sangwan, M. R. Wasielewski, M. C. Hersam, G. C. Schatz, D. M. DeLongchamp, A. Facchetti, T. J. Marks, *Energy Environ. Sci.* **2022**, *15*, 645.
[20] J. Guo, B. Qiu, D. Yang, C. Zhu, L. Zhou, C. Su, U. S. Jeng, X. Xia, X. Lu, L. Meng, Z. Zhang, Y. Li, *Adv. Funct. Mater.* **2022**, *32*, 2110159.
[21] X. Gu, Y. Wei, G. Lu, Z. Han, D. Zheng, G. Lu, J. Zhang, Z. Wei, Y. Cai, X. Zhang, H. Huang, *Aggregate* **2023**, *4*, e388.
[22] Q. Shen, C. He, S. Li, L. Zuo, M. Shi, H. Chen, *Acc. Mater. Res.* **2022**, *3*, 644.
[23] D. Luo, C. J. Brabec, A. K. K. Kyaw, *Nano Energy* **2023**, *114*, 108661.
[24] A. Mishra, G. D. Sharma, *Angew. Chem., Int. Ed.* **2023**, *62*, 202219245.
[25] K. Xian, R. Ma, K. Zhou, J. Liu, M. Gao, W. Zhao, M. Li, Y. Geng, L. Ye, *Aggregate* **2024**, *5*, e466.
[26] G. Wang, L.-W. Feng, W. Huang, S. Mukherjee, Y. Chen, D. Shen, B. Wang, J. Strzalka, D. Zheng, F. S. Melkonyan, *Proc. Natl. Acad. Sci. USA* **2020**, *117*, 17551.
[27] H. Zhao, J. Xue, H. Wu, B. Lin, Y. Cai, K. Zhou, D. Yun, Z. Tang, W. Ma, *Adv. Funct. Mater.* **2023**, *33*, 2210534.
[28] Y. Cai, C. Xie, Q. Li, C. Liu, J. Gao, M. H. Jee, J. Qiao, Y. Li, J. Song, X. Hao, H. Y. Woo, Z. Tang, Y. Zhou, C. Zhang, H. Huang, Y. Sun, *Adv. Mater.* **2023**, *35*, 2208165.
[29] H. Liang, X. Bi, H. Chen, T. He, Y. Lin, Y. Zhang, K. Ma, W. Feng, Z. Ma, G. Long, C. Li, B. Kan, H. Zhang, O. A. Rakitin, X. Wan, Z. Yao, Y. Chen, *Nat. Commun.* **2023**, *14*, 4707.
[30] N. Camaioni, C. Carbonera, L. Ciammaruchi, G. Corso, J. Mwaura, R. Po, F. Tinti, *Adv. Mater.* **2023**, *35*, 2210146.
[31] F. Zhao, D. He, C. Zou, Y. Li, K. Wang, J. Zhang, S. Yang, Y. Tu, C. Wang, Y. Lin, *Adv. Mater.* **2023**, *35*, 2210463.
[32] X. Duan, C. Liu, Y. Cai, L. Ye, J. Xue, Y. Yang, W. Ma, Y. Sun, *Adv. Mater.* **2023**, *35*, 2302927.
[33] X. Song, H. Xu, X. Jiang, S. Gao, X. Zhou, S. Xu, J. Li, J. Yu, W. Liu, W. Zhu, P. Müller-Buschbaum, *Energy Environ. Sci.* **2023**, *16*, 3441.
[34] C. Xie, X. Zeng, C. Li, X. Sun, S. Liang, H. Huang, B. Deng, X. Wen, G. Zhang, P. You, C. Yang, Y. Han, S. Li, G. Lu, H. Hu, N. Li, Y. Chen, *Energy Environ. Sci.* **2024**, *17*, 2441.
[35] D. Luo, Z. Jiang, W. L. Tan, L. Zhang, L. Li, C. Shan, C. R. McNeill, P. Sonar, B. Xu, A. K. K. Kyaw, *Adv. Energy Mater.* **2023**, *13*, 2203402.
[36] T. A. Dela Peña, R. Ma, Y. Luo, Z. Xing, Q. Wei, Y. Hai, Y. Li, S. A. Garcia, K. L. Yeung, T. Jia, K. S. Wong, H. Yan, G. Li, M. Li, J. Wu, *Adv. Energy Mater.* **2024**, *14*, 2303169.
[37] L. Ma, Y. Xu, Y. Zu, Q. Liao, B. Xu, C. An, S. Zhang, J. Hou, *Sci. China Chem* **2020**, *63*, 21.

[38] J. Gao, X. Ma, C. Xu, X. Wang, J. H. Son, S. Y. Jeong, Y. Zhang, C. Zhang, K. Wang, L. Niu, J. Zhang, H. Y. Woo, J. Zhang, F. Zhang, *Chem. Eng. J.* **2022**, *428*, 129276.
[39] L. Zhang, S. Yang, B. Ning, F. Yang, W. Deng, Z. Xing, Z. Bi, K. Zhou, Y. Zhang, X. Hu, *Sol. RRL* **2022**, *6*, 2100838.
[40] J. Lee, D. H. Sin, B. Moon, J. Shin, H. G. Kim, M. Kim, K. Cho, *Energy Environ. Sci.* **2017**, *10*, 247.
[41] L. Zhang, L. Hu, X. Wang, H. Mao, L. Zeng, L. Tan, X. Zhuang, Y. Chen, *Adv. Funct. Mater.* **2022**, *32*, 2202103.
[42] R. Sun, T. Wang, X. Yang, Y. Wu, Y. Wang, Q. Wu, M. Zhang, C. J. Brabec, Y. Li, J. Min, *Nat. Energy* **2022**, *7*, 1087.
[43] H. Fu, Z. Peng, Q. Fan, F. R. Lin, F. Qi, Y. Ran, Z. Wu, B. Fan, K. Jiang, H. Y. Woo, G. Lu, H. Ade, A. K. Y. Jen, *Adv. Mater.* **2022**, *34*, 2202608.
[44] B. Zhang, F. Yang, S. Chen, H. Chen, G. Zeng, Y. Shen, Y. Li, Y. Li, *Adv. Funct. Mater.* **2022**, *32*, 2202011.
[45] H. Ning, Q. Jiang, P. Han, M. Lin, G. Zhang, J. Chen, H. Chen, S. Zeng, J. Gao, J. Liu, F. He, Q. Wu, *Energy Environ. Sci.* **2021**, *14*, 5919.
[46] D.-H. Lee, Y. M. Yang, J. You, E. Richard, G. Li, *Nanotechnology* **2014**, *25*, 295401.
[47] R. Gui, K. Xian, Y. Shi, W. Zhang, J. Qiao, Z. Fu, J. Wang, F. Cui, Q. Wang, V. K. Wong, P. Lu, S. K. So, M. Zhang, L. Ye, G. Li, X. Hao, H. Yin, *Adv. Energy Mater.* **2023**, *13*, 2302029.
[48] Y. Yang, E. Feng, H. Li, Z. Shen, W. Liu, J. Guo, Q. Luo, J. Zhang, G. Lu, C. Ma, J. Yang, *Nano Res.* **2021**, *14*, 4236.
[49] Y. Xie, C. Zhou, X. Ma, S. Y. Jeong, H. Y. Woo, F. Huang, Y. Yang, H. Yu, J. Li, F. Zhang, K. Wang, X. Zhu, *Adv. Energy Mater.* **2024**, *14*, 2400013.
[50] C. He, Y. Pan, G. Lu, B. Wu, X. Xia, C.-Q. Ma, Z. Chen, H. Zhu, X. Lu, W. Ma, L. Zuo, H. Chen, *Adv. Mater.* **2022**, *34*, 2203379.
[51] Y. Wang, J. Xue, H. Zhong, C. R. Everett, X. Jiang, M. A. Reus, A. Chumakov, S. V. Roth, M. A. Adedeji, N. Jili, K. Zhou, G. Lu, Z. Tang, G. T. Mola, P. Müller-Buschbaum, W. Ma, *Adv. Energy Mater.* **2023**, *13*, 2203496.
[52] L. Wen, H. Mao, L. Zhang, J. Zhang, Z. Qin, L. Tan, Y. Chen, *Adv. Mater.* **2024**, *36*, 2308159.
[53] J. Wang, C. Han, S. Wen, F. Bi, Z. Hu, Y. Li, C. Yang, X. Bao, J. Chu, *Energy Environ. Sci.* **2023**, *16*, 2327.
[54] Y. Zhang, K. Liu, J. Huang, X. Xia, J. Cao, G. Zhao, P. W. K. Fong, Y. Zhu, F. Yan, Y. Yang, X. Lu, G. Li, *Nat. Commun.* **2021**, *12*, 4815.
[55] Y. Cai, Q. Li, G. Lu, H. S. Ryu, Y. Li, H. Jin, Z. Chen, Z. Tang, G. Lu, X. Hao, H. Y. Woo, C. Zhang, Y. Sun, *Nat. Commun.* **2022**, *13*, 2369.
[56] Y. Zhang, W. Deng, C. E. Petoukhoff, X. Xia, Y. Lang, H. Xia, H. Tang, H. T. Chandran, S. Mahadevan, K. Liu, P. W. K. Fong, Y. Luo, J. Wu, S.-W. Tsang, F. Laquai, H. Wu, X. Lu, Y. Yang, G. Li, *Joule* **2024**, *8*, 509.
[57] D. Li, H. Zhang, X. Cui, Y.-N. Chen, N. Wei, G. Ran, H. Lu, S. Chen, W. Zhang, C. Li, Y. Liu, Y. Liu, Z. Bo, *Adv. Mater.* **2024**, *36*, 2310362.
[58] L. Ma, S. Zhang, J. Zhu, J. Wang, J. Ren, J. Zhang, J. Hou, *Nat. Commun.* **2021**, *12*, 5093.
[59] Z. Han, C. e. Zhang, T. He, J. Gao, Y. Hou, X. Gu, J. Lv, N. Yu, J. Qiao, S. Wang, C. Li, J. Zhang, Z. Wei, Q. Peng, Z. Tang, X. Hao, G. Long, Y. Cai, X. Zhang, H. Huang, *Angew. Chem., Int. Ed.* **2024**, *63*, 202318143.
[60] Y. Zhou, M. Li, H. Lu, H. Jin, X. Wang, Y. Zhang, S. Shen, Z. Ma, J. Song, Z. Bo, *Adv. Funct. Mater.* **2021**, *31*, 2101742.
[61] X. Wang, R. Zeng, H. Lu, G. Ran, A. Zhang, Y.-N. Chen, Y. Liu, F. Liu, W. Zhang, Z. Tang, Z. Bo, *Chin. J. Chem.* **2023**, *41*, 665.
[62] Q. Liu, Y. Jiang, K. Jin, J. Qin, J. Xu, W. Li, J. Xiong, J. Liu, Z. Xiao, K. Sun, S. Yang, X. Zhang, L. Ding, *Sci. Bull.* **2020**, *65*, 272.
[63] Z. Zhong, S. Chen, J. Zhao, J. Xie, K. Zhang, T. Jia, C. Zhu, J. Jing, Y. Liang, L. Hong, S. Zhu, D. Ma, F. Huang, *Adv. Energy Mater.* **2023**, *13*, 2302273.
[64] X. Zhong, T.-W. Chen, L. Yan, W. You, *ACS Appl. Polym. Mater.* **2023**, *5*, 1937.
[65] D. Li, N. Deng, Y. Fu, C. Guo, B. Zhou, L. Wang, J. Zhou, D. Liu, W. Li, K. Wang, Y. Sun, T. Wang, *Adv. Mater.* **2023**, *35*, 2208211.
[66] R. Ma, H. Li, T. A. Dela Peña, X. Xie, P. W.-K. Fong, Q. Wei, C. Yan, J. Wu, P. Cheng, M. Li, G. Li, *Adv. Mater.* **2024**, *36*, 2304632.
[67] Y. Ma, S. Luan, D. Cai, S.-Q. Zhang, J.-Y. Wang, Q. Tu, Y. Zhu, Q. Zheng, *Aggregate* **2023**, *4*, e322.
[68] J. Rivnay, S. C. B. Mannsfeld, C. E. Miller, A. Salleo, M. F. Toney, *Chem. Rev.* **2012**, *112*, 5488.
[69] W. Gao, R. Ma, T. A. Dela Peña, C. Yan, H. Li, M. Li, J. Wu, P. Cheng, C. Zhong, Z. Wei, A. K. Y. Jen, G. Li, *Nat. Commun.* **2024**, *15*, 1946.
[70] X. Jiang, A. J. Gillett, T. Zheng, X. Song, J. E. Heger, K. Sun, L. V. Spanier, R. Guo, S. Liang, S. Bernstorff, P. Müller-Buschbaum, *Energy Environ. Sci.* **2023**, *16*, 5970.
[71] R. Ma, Q. Fan, T. A. Dela Peña, B. Wu, H. Liu, Q. Wu, Q. Wei, J. Wu, X. Lu, M. Li, W. Ma, G. Li, *Adv. Mater.* **2023**, *35*, 2212275.
[72] L. Chen, R. Ma, J. Yi, T. A. Dela Peña, H. Li, Q. Wei, C. Yan, J. Wu, M. Li, P. Cheng, H. Yan, G. Zhang, G. Li, *Aggregate* **2024**, *5*, e455.
[73] Y. Liu, Y. Jin, Y. Wu, Y. Zhong, *J. Mater. Chem. C* **2022**, *10*, 13646.
[74] Y.-F. Shen, H. Zhang, J. Zhang, C. Tian, Y. Shi, D. Qiu, Z. Zhang, K. Lu, Z. Wei, *Adv. Mater.* **2023**, *35*, 2209030.
[75] N. Schopp, H. M. Luong, B. R. Luginbuhl, P. Panoy, D. Choi, V. Promarak, V. V. Brus, T.-Q. Nguyen, *ACS Energy Lett.* **2022**, *7*, 1626.
[76] Y. Tamai, Y. Murata, S.-i. Natsuda, Y. Sakamoto, *Adv. Energy Mater.* **2024**, *14*, 2301890.
[77] T. A. Dela Peña, R. Ma, Z. Xing, Q. Wei, J. I. Khan, R. M. Young, Y. Hai, S. A. Garcia, X. Zou, Z. Jin, F. L. Ng, K. L. Yeung, D. F. Swearer, M. R. Wasielewski, J. Wang, H. Cha, H. Yan, K. S. Wong, G. Li, M. Li, J. Wu, *Energy Environ. Sci.* **2023**, *16*, 3416.
[78] A. K. Ko Kyaw, D. Gehrig, J. Zhang, Y. Huang, G. C. Bazan, F. Laquai, T.-Q. Nguyen, *J. Mater. Chem. A* **2015**, *3*, 1530.
[79] M. Du, A. Tang, J. Yu, Y. Geng, Z. Wang, Q. Guo, Y. Zhong, S. Lu, E. Zhou, *Adv. Energy Mater.* **2023**, *13*, 2302429.
[80] F. Sun, X. Zheng, T. Hu, J. Wu, M. Wan, Y. Xiao, T. Cong, Y. Li, B. Xiao, J. Shan, E. Wang, X. Wang, R. Yang, *Energy Environ. Sci.* **2024**, *17*, 1916.
[81] B. Siegmund, M. T. Sajjad, J. Widmer, D. Ray, C. Koerner, M. Riede, K. Leo, I. D. W. Samuel, K. Vandewal, *Adv. Mater.* **2017**, *29*, 1604424.
[82] W. Yang, W. Wang, Y. Wang, R. Sun, J. Guo, H. Li, M. Shi, J. Guo, Y. Wu, T. Wang, *Joule* **2021**, *5*, 1209.
[83] Y. Gao, Y. Yu, J. Guo, R. Sun, T. Wang, W. Wang, J. Min, *Adv. Opt. Mater.* **2023**, *11*, 2202685.